Turkish Journal of Physics

http://journals.tubitak.gov.tr/physics/

Research Article

Turk J Phys
(2020) 44: 67 – 76

doi:10.3906/fiz-1909-17

Magnetic properties of Mn doped crystalline and amorphous Ge thin films grown on Si (111)

İlknur GÜNDÜZ AYKAÇ[1,2], Aykut Can ÖNEL[1], Burcu TOYDEMİR YAŞASUN[1], Leyla ÇOLAKEROL ARSLAN[1,3,*]

[1]Department of Physics, Gebze Technical University, Kocaeli, Turkey
[2]Department of Engineering Physics, İstanbul Medeniyet University, İstanbul, Turkey
[3]Nanotechnology Institute, Gebze Technical University, Kocaeli, Turkey

Received: 26.09.2019 • **Accepted/Published Online:** 28.01.2020 • **Final Version:** 12.02.2020

Abstract: We investigated the effects of crystalline order on the structural and magnetic properties of ultrathin Mn-doped Ge thin films grown by thermal diffusion. The dopant motion which occurs during the annealing stage appears to differ considerably depending upon whether the Ge layer is in a crystalline or an amorphous state. The details of the temperature-dependent magnetization curves reveal that the a-MnGe and c-MnGe films show ferromagnetic property up to 300K and ~250K, respectively. Ferromagnetic Mn_5Ge_3 thin film with weakly anisotropic in-plane magnetization is formed on amorphous Ge thin film, while weakly ferromagnetic $Mn_5Ge_xSi_{3-x}$ nanostructures are developed on crystalline Ge thin film due to diffusion of Mn atoms through the Ge layer and interact with Si substrate.

Key words: Mn-Ge ferromagnetism, solid phase epitaxy, X-ray photoelectron spectroscopy depth profiling

1. Introduction

Transition metal doped germanium based diluted magnetic semiconductors are of significant scientific and technological interest due to their use in semiconductor-based spintronic devices such as magneto-optoelectronic devices, spin field-effect transistors, and spin logic devices [1–3]. Out of all the transition metals, Mn is the most favourable dopant because Mn ions have the highest possible magnetic moment in Ge if placed at the substitutional sites [4]. However, due to the low solubility of Mn in Ge [5], substitutional Mn doping is very difficult. The majority of Mn doped Ge films reported to date contain different magnetic phases and precipitates depending on the distribution of Mn atoms in Ge, which is mainly governed by Mn diffusion mechanism during growth procedure [6,7]. Ion implantation and low temperature synthesis techniques with very low doping concentration are highly desirable to minimize precipitate formation, but the main disadvantage of these growth processes is the large number of defects that are introduced during growth [8–11]. Since the defects produce local lattice distortions, the position of Mn atoms around the defects is different from their crystallographic equilibrium positions. Consequently, the exchange interactions between Mn atoms around the defects lead to different magnetic coupling. The local environment and degree of disorder in amorphous Ge is very different from that of crystalline Ge, and the magnetic moment of Mn atoms is extremely sensitive to the local environment. A comparative experimental study on the local structures and magnetic interactions of Mn atoms in crystalline and amorphous Ge is important to understand the effect of defects on the distribution

*Correspondence: lcolakerol@gtu.edu.tr

mechanism of dopants. Despite past intensive studies, controversial issues still remain in the distribution of magnetic moments in Mn-doped crystalline and amorphous Ge thin films [12–16]. We have applied a surface driven approach for the incorporation of Mn into Ge. This approach has been used with Mn doped GaN and GaAs thin films in achieving room temperature ferromagnetism, which is high compared to that of traditional diluted magnetic semiconductors [17,18]. This work presents a systematic study of the magnetic properties of Mn-doped amorphous (a-MnGe) and crystalline (c-MnGe) Ge films prepared by solid phase epitaxy where Mn is deposited on Ge at room temperature, and subsequently annealed at elevated temperature. A thermal diffusion doping technique has been chosen so that the films can be prepared with quite controllable atomic composition without causing any crystal damage. The aim of the experiment is to reveal possible interactions between Mn atoms in Ge as well as related changes in the magnetic properties of a-MnGe and c-MnGe systems. Since the densities and the chemical states of the thermally diffused ions vary as a function of the depth, it is important to investigate the depth profile of atomic distribution and chemical bonding of the diffused ions. In order to understand the diffusion behaviour of Mn atoms, we have employed X-ray photoelectron spectroscopy (XPS) depth profile analysis. By measuring the magnetization and the magnetic anisotropy through vibrating sample magnetometer (VSM) and electron spin resonance (ESR), we have assessed the contribution of Mn dopants to the magnetic behaviour of the films. Results indicate that a-MnGe film shows clear room temperature ferromagnetism and the magnetic interactions weaken with the increasing crystalline order.

2. Experimental

Mn-doped Ge films were deposited via molecular beam epitaxy (MBE) onto n-type Si (111) substrates. Si substrates were rinsed in a 1:10 solution of concentrated HF and deionized water firstly and then annealed in ultrahigh vacuum at 650 °C for several hours and monitored by means of low energy electron diffraction (LEED) until a well-ordered 7 $\times$7 reconstruction appeared. Both amorphous and crystalline Ge films with thickness of 50 nm were then deposited by molecular beam epitaxy at temperatures of 90 °C and 480 °C, respectively. Next, a 3 nm Mn layer was deposited at room temperature. Subsequently, both films were annealed for 20 min at 400 °C. Deposition rates of Ge and Mn were monitored by a quartz crystal microbalance. The structure and the crystallinity of the deposited films were examined by a Rigaku SmartLab X-ray diffractometer (XRD) which uses Cu Kα radiation (λ = 1.54178 Å). XPS spectra of the films were collected using a SPECS PHOIBOS 100 hemispherical analyser under a base vacuum of less than 1 $\times 10^{-10}$ Torr, where an Al Kα X-ray (hν = 1486.6 eV) was used as the excitation source. The energy scale of the spectrometer was calibrated by setting the measured Au 4$f_{7/2}$ binding energy to 84 eV with regard to Fermi energy. Depth profile XPS study was performed by etching the surface by a 3 kV Ar+ ion beam ions for 10 min repeatedly and XPS spectra were taken after each etching cycle. XPS analysis was continued until no Mn signal was detected. Quantification was performed after a Shirley background subtraction using core-line peak areas and the tabulated sensitivity factors for the instrument. The magnetic measurements were carried out using VSM in the temperature range from 10K to 350K. For obtaining information on the magnetic anisotropy of MnGe films, ESR measurements were performed at temperatures from 300K down to 150K using an X-band JEOL JES-FA 300 spectrometer equipped by an electromagnet which provides a DC magnetic field up to 2 kG in the horizontal plane.

3. Results

Figure 1 shows the X-ray diffraction patterns of a-MnGe and c-MnGe thin films deposited on Si (111) substrates at 90 °C and 480 °C. The sharp peaks at 28°and 95°are attributed to silicon substrate (111) and (333) reflections,

respectively. A broad hump on the left shoulder of Si (111) peak obtained from a-MnGe film is attributed to diffuse scattering from randomly ordered atomic layers and indicative of amorphous film. On the other hand, the c-MnGe film grown at 480 °C has sharp Ge (111) and Ge (333) crystalline peaks. Note that the lattice parameter obtained from the position of (111) Ge peak is 5.66 Å. This indicates that Mn doping in Ge lattice did not affect the atomic distance. Moreover, there are no traces of secondary phases in the XRD spectrum.

XPS measurements were performed to determine the composition and the chemical state of Mn in the films. XPS analysis of Mn 2p spectra of the films shows that after the deposition of Mn at room temperature, metallic Mn is formed in both films. The Mn 2p spectra of a-MnGe and c-MnGe taken after annealing process are shown in Figure 2 and display 2 spin-orbit doublets with lower and higher energies, which can be assigned to the binding energies of Mn $2p_{1/2}$ and Mn $2p_{3/2}$, respectively. The first doublets at 638.8 and 649.8 eV and the second doublets at 639.9 and 650.9 eV are ascribed to metallic Mn and metallic manganese phases such as Mn_5Ge_3 [19] and $Mn_5Ge_{3-x}Si_x$ [20], respectively. It should be noted that the binding energies of Mn 2p related peaks in c-MnGe were negatively shifted compared to those of Mn 2p in a-MnGe, and the intensity of the higher energy component is stronger than that in a-MnGe. The latter result is good proof that a higher portion of Mn on the surface of amorphous Ge forms metallic manganese phase during the annealing process. The spin-orbit splitting energy (Δso) value for both films is 11 eV. This energy splitting is lower than that of metallic Mn (11.4) [19]. The decrease of spin-orbit splitting energy indicates that the Mn detected in the films is probably in the cluster form. The narrowing effect of metal cluster size on the energy splitting has been observed in various metal clusters [21]. This is in line with the presence of Mn clusters in Ge. We also note that there is a slight broadening of the higher energy peak of c-MnGe compared to that for a-MnGe, indicating the presence of inhomogeneously distributed clusters inside the c-MnGe film.

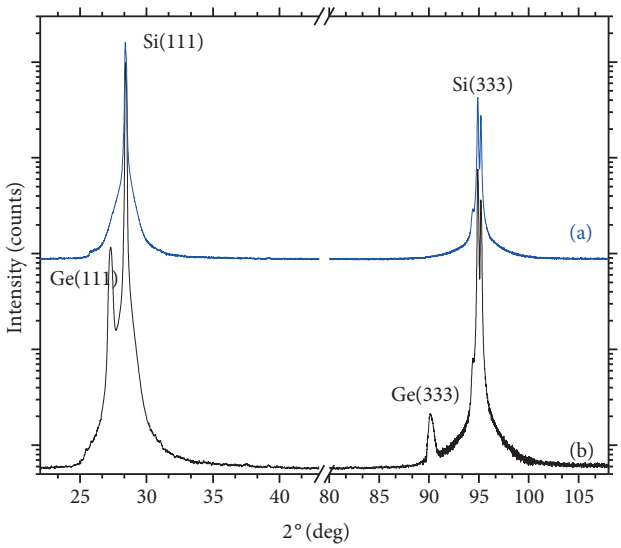

Figure 1. XRD patterns of amorphous and crystalline MnGe films.

XPS depth profiles of a-MnGe and c-MnGe are shown in Figures 3a and 3b, respectively. The sputter-depth profiling shows that significant Mn diffusion occurred for c-MnGe and was effectively suppressed for a-MnGe film. For a-MnGe, the Ge signal increases and Mn signal decreases dramatically with the sputtering time of 10 min, indicating that a high atomic concentration of Mn atoms accumulates at the surface during

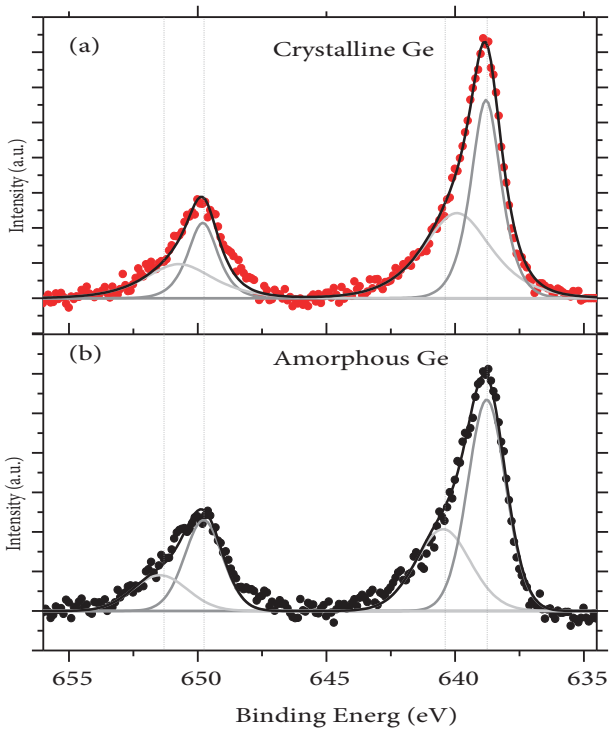

Figure 2. Mn 2p XPS spectra of c-MnGe (upper panel) and a-MnGe (lower panel): experimental data (circles) are shown together with the results of the peak fitted data (black line).

the annealing process and these Mn dopants interact with Ge atoms. The atomic percentage of Ge and Mn more or less remains constant up to the point where the Si surface is reached, indicating uniform depth distribution of Mn inside a-MnGe film. In contrast, the depth profile of c-MnGe in Figure 3b shows a detectable interdiffusion between Mn and Si layers. The appearance of the Si signal before etching procedure indicates that Ge heteroepitaxially grows on Si in an island growth mode, which was also confirmed by subsequent atomic force microscopy (AFM) results. For low Ge thicknesses, we have shown the formation of domed shaped Ge islands on Si in our previous studies by TEM investigations [22]. At the Ge/Si interface, Mn content increased to about 13%. This proves that Mn atoms penetrate into the Si substrate either through the exposed regions between Ge islands or through the Ge islands. Kassim et al. have reported similar observations for MnGe quantum dots, where more Mn was present underneath the Ge superdomes than on the surface [23].

In order to cross check the surface morphologies, the surfaces of MnGe films were analysed by AFM (Figure 4). The images of the MnGe films were acquired in a 10 µm ×10 µm area. The a-MnGe film was observed to have a smooth surface (RMS roughness of 2.8 nm). The surface texture appears due to the low diffusion length of Ge atoms on Si at 90 °C [24]. On the other hand, a typical island growth of MnGe grains formed on the c-MnGe surface. Due to the heteroepitaxial growth and large lattice mismatch between Si and Ge, a large density of big isolated Ge islands is formed on Si surface. The corresponding RMS roughness is 9.84 nm for c-MnGe.

To probe the magnetic behaviour of the MnGe films, field and temperature-dependent magnetization measurements were performed using the VSM system. Figure 5 shows the variation of magnetization with the applied magnetic field (M–H curves) measured at different temperatures from 10K to 300K. Notably, the

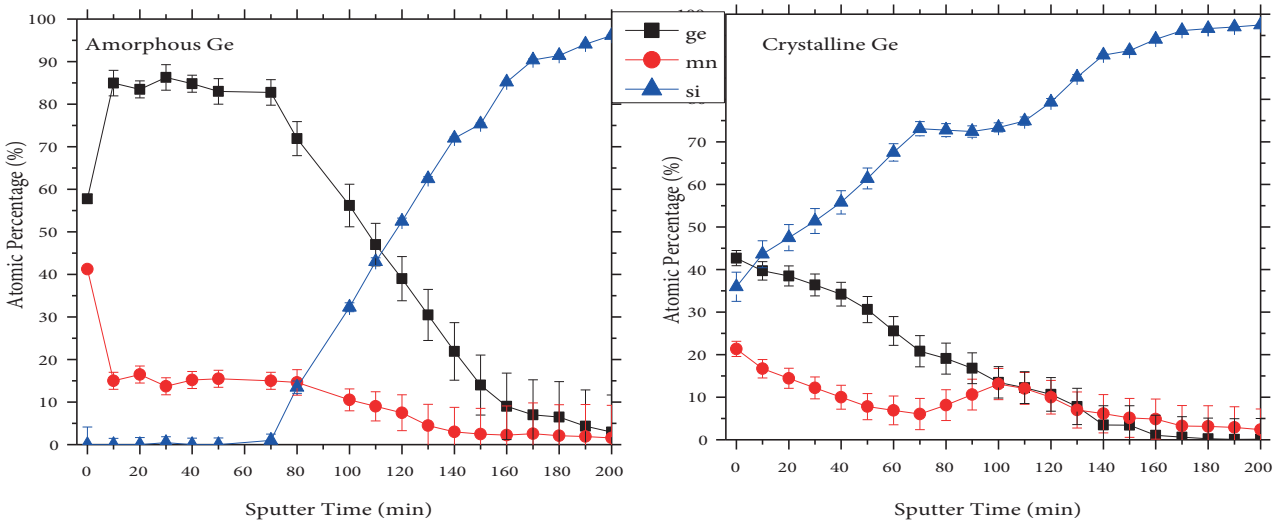

Figure 3. The XPS depth profiles of (a) amorphous MnGe and (b) crystalline MnGe films using 3 keV Ar^+ ion beam.

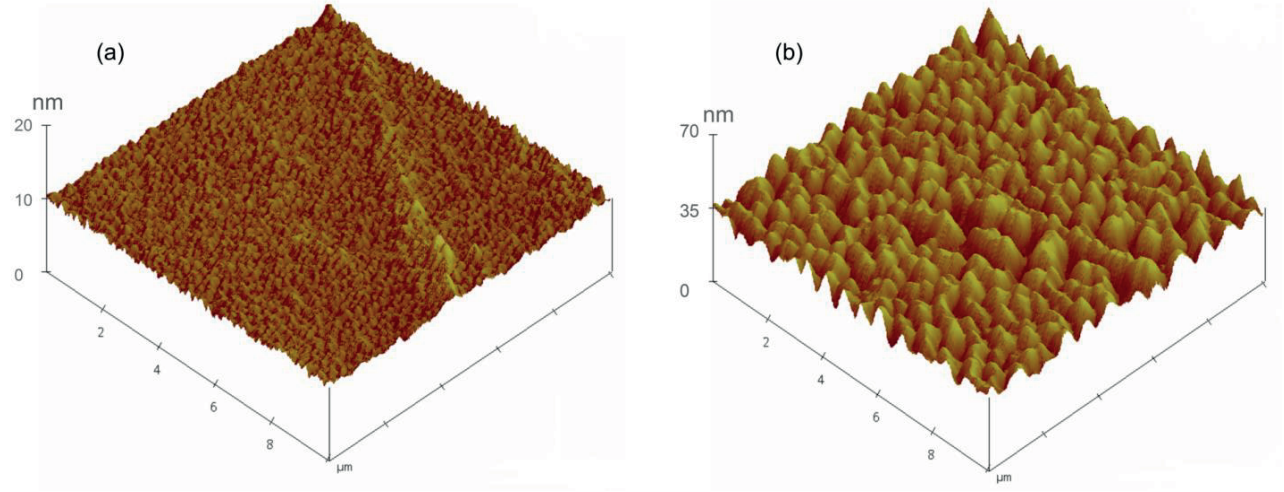

Figure 4. 3-dimensional AFM images of (a) amorphous MnGe and (b) crystalline MnGe films.

a-MnGe and c-MnGe films no longer exhibit any hysteresis or remanence above 300K and 250K, respectively. The diamagnetic contribution of the Si substrate, which is determined from M–H data taken at 350K, is subtracted from all magnetization curves. Upon cooling down to 10K, an obvious increase in the coercivity and the magnetization were observed. Particularly, the hysteresis still did not reach saturation at 0.8T with the magnetization of 120 emu cm^{-3} and 60 emu cm^{-3} for a-MnGe and c-MnGe, respectively. It must be emphasized that the temperature dependences for the 2 samples are also different: the magnetization measured at 100 mT shows that zero-field cooling ZFC and field cooling FC curves of the a-MnGe superimpose from 10K to 350K (Figure 6), whereas in contrast, the crystalline sample exhibits a large divergence between the ZFC and FC data. The c-MnGe exhibits a bifurcation below 250K and also a broad plateau near 210K corresponding to average blocking temperature T_B. Below the T_B, the ZFC magnetization stays constant down to 70K, whereas there is a gradual increase in the FC magnetization. The slight increase of the magnetic moment at low

temperatures is due to the presence of magnetically disordered frozen surface spins, which are also responsible for the lack of saturation at low temperatures. The temperature dependence of the coercive field (H_c) and the reduced remanence M_r/M_s, where Mr is the remanent magnetization and Ms is the saturation magnetization, for c-MnGe film are shown in the inset in Figure 5. The H_c decreases monotonically along with the increase of the temperature. However, M_r/M_s remains nearly constant at 0.4 for T <150K and decreases with increasing temperature. The low temperature value of M_r/M_s is close to the typical value (0.5) for randomly oriented magnetic nanoparticles with a uniaxial anisotropy. The lower values are accompanied by large average particle size and the variation in the size distribution induces higher blocking temperature and a broadening of the ZFC curve. These observations suggest the existence of superparamagnetic interactions in the sample of c-MnGe. Nevertheless, a-MnGe and c-MnGe samples exhibit ferromagnetic coupling with Curie temperature (defined as the peak of dM/dT in the M vs. T curve) of 300K and 243K, respectively.

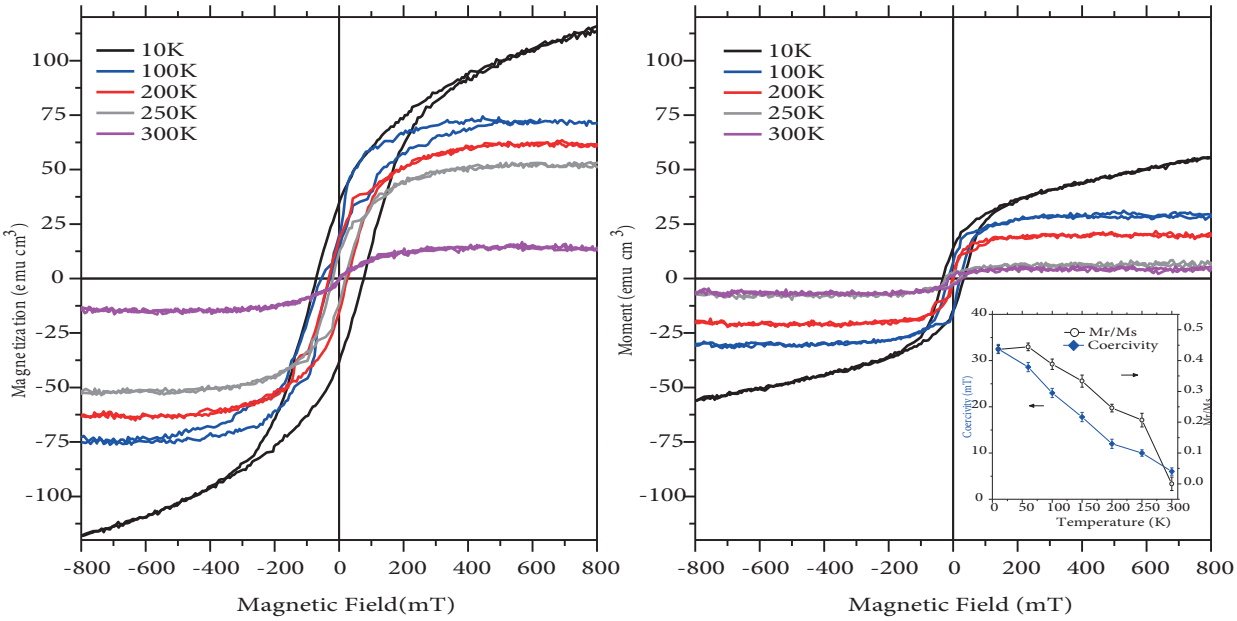

Figure 5. The magnetic hysteresis loops measured by VSM at various temperatures for (a) amorphous MnGe and (b) crystalline MnGe films. Inset: The temperature dependence of the coercive field (Hc) and the reduced remanence M_r/M_s for c-MnGe film.

It can clearly be seen that the saturation magnetization and magnetic transition temperature change depending on the crystal quality of Ge layer. These differences can be caused by the formation of secondary phases ($Mn_5Ge_{3-x}Si_x$) inside the samples. Although we could not observe any XRD peak associated with secondary phases, magnetic properties and XPS results of the amorphous film show clear evidence of Mn_5Ge_3 phase formation. For the a-MnGe sample, the overlapping of FC and ZFC magnetization indicates the growth and development of large magnetic domains of single Mn_5Ge_3 phase, which is consistent with the Curie temperature [25]. For the crystalline sample, the difference between FC and ZFC curves in a large temperature range (below 220K) suggests the presence of short range magnetic ordering within the nanodomains. Considering XPS results, Mn atoms diffuse through Ge into the Si lattice or stay above Ge layer as metallic Mn. This behaviour is related to the change in the electronic environment as replacing Ge ($3d^{10}4s^24p^2$) by Si ($3s^23p^2$) and is expected to influence the magnetic structures of the $Mn_5Ge_{3-x}Si_x$ compound. In previous studies,

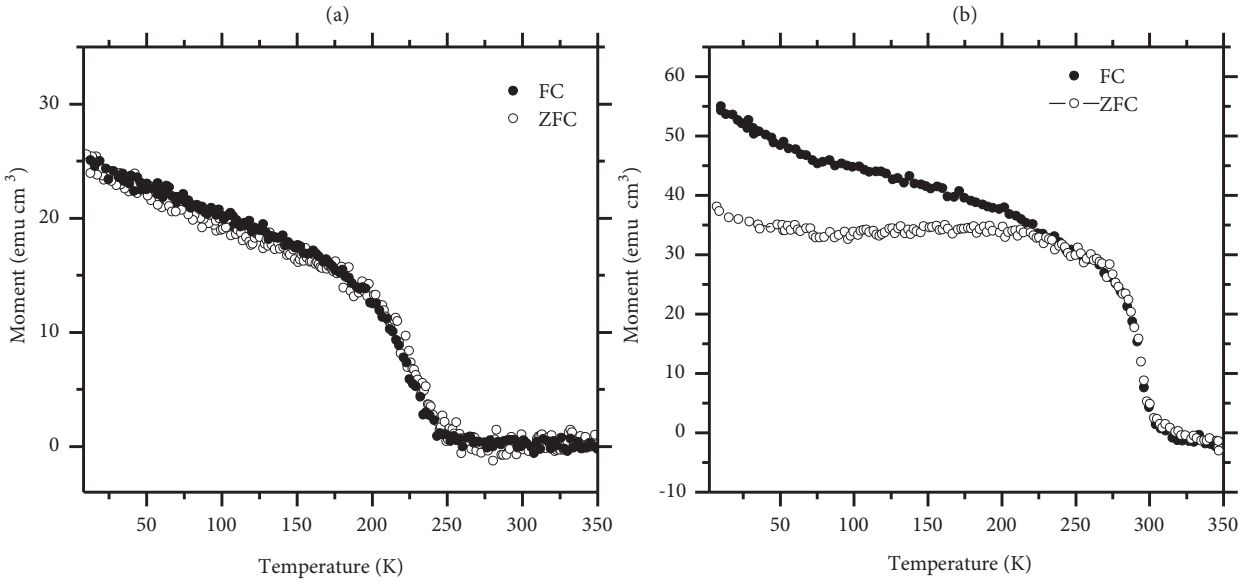

Figure 6. M (T) curves for (a) amorphous MnGe and (b) crystalline MnGe (H = 100 mT).

Curie temperature of $Mn_5Ge_{3-x}Si_x$ structure was found to change between 298K and 252 K depending on the x value within x = 0–1.5 [26,27]. Therefore, it is seen that the transition temperature is a reasonable value that can be reached by incorporating Si into the structure. However, the Curie temperature, which is slightly out of the limits mentioned above, can be reached on $Mn_5Ge_{3-x}Si_x$ compound with x value greater than 1.5, so that the Si concentration in the nanomagnetic domains is higher than the Ge concentration. To determine the nature of magnetic ordering and the magnetic anisotropy of a-MnGe film, a series of angular and temperature-dependent FMR experiments were carried out as shown in Figure 7. It should be noted that no distinguishable FMR signal was detected for c-MnGe. The absence of an FMR spectrum for c-MnGe can be explained by the smaller size and density of ferromagnetic $Mn_5Ge_{3-x}Si_x$ grains and low degree of ferromagnetic ordering among them. FMR spectra that are presented in Figure 7a show the angular dependence of the externally applied field in the sample plane at room temperature. A single FMR peak with a small uniaxial anisotropy with the hard axis perpendicular to film surface is observed. This indicates that the FMR resonance field is dominated by the magnetic shape anisotropy field since the sample is a thin film, consistent with the previous works on Mn_5Ge_3 thin films [28,29]. Figure 7b shows the temperature dependence of the FMR spectra with the magnetic field applied in the in-plane direction. As can be seen from the inset, with the effective g-value calculated using the equation of $g = h\nu/\beta H_{res}$ (where ν = 9.1 GHz, h is the Planck constant, β is the Bohr magnetron) fields and the resonance line width rise gradually below Curie temperature with the decrease of temperature. It is seen from the figure that the values of g-factor vary from 2.04 above Curie temperature to 5.1 at 260K. The increase of g-factor with the decrease of temperature indicates a surface contribution to magnetic interactions. Considering the low thickness of the film (5 nm), the magnetization on the surface is comparable to the bulk and the interaction of both leads to temperature-dependent shift of the FMR line to lower fields [30]. It has been known that strong spin-orbit coupling can cause higher values of g-factors in ferromagnetic nanostructures and thin films [31,32]. The reason for obtaining such g factors could be due to the generation of orbital magnetic moment at the surface which enhances the effective spin-orbit coupling.

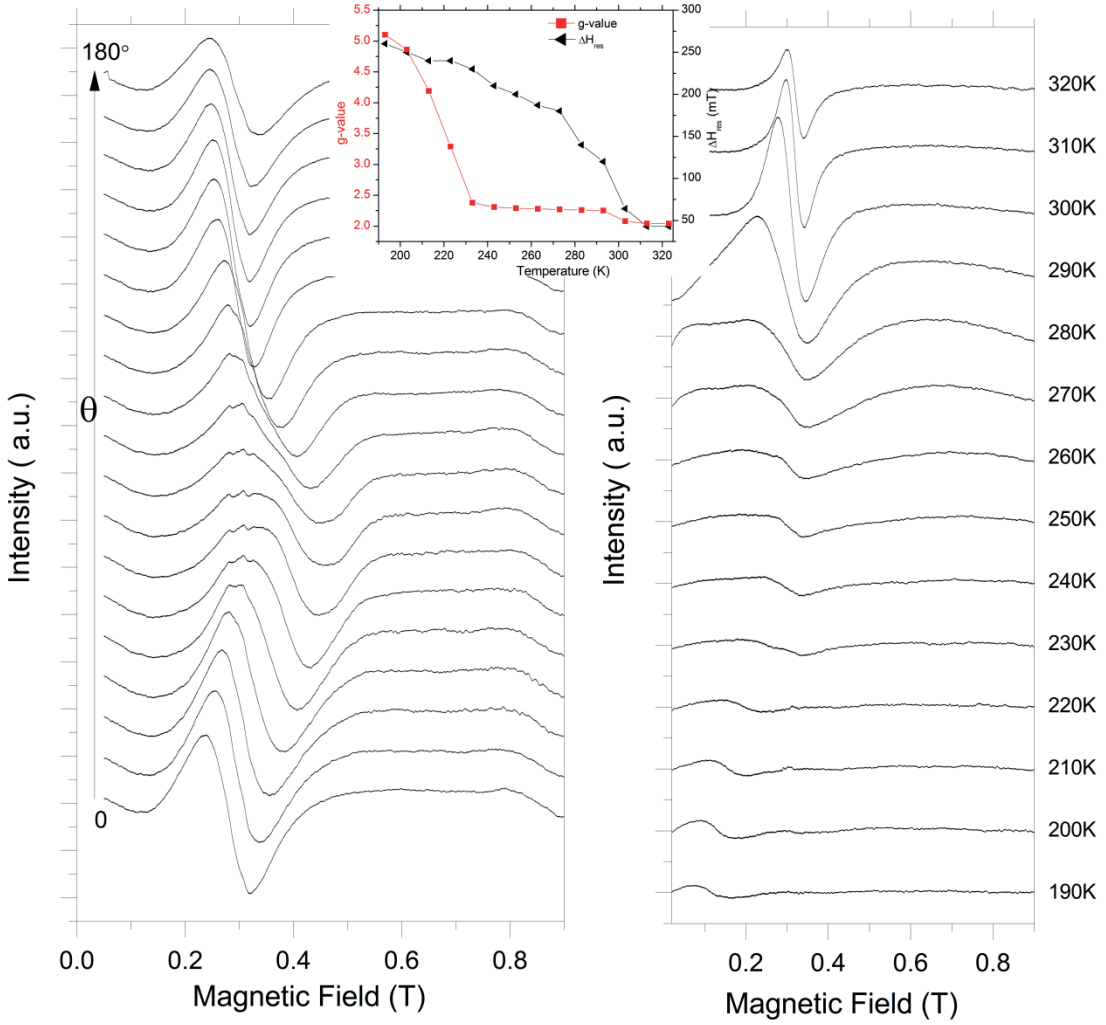

Figure 7. (a) Angular dependence of FMR fields for a-MnGe film at 300K. (b) Temperature dependence of FMR spectra for a-MnGe film for the magnetic field in the plane orientation. Inset shows the temperature dependence of the g-value and resonance line width ΔH_{res}.

4. Conclusion

In conclusion, we demonstrated that Mn atom distribution and corresponding magnetic properties inside thin Ge film depend on the structural properties of Ge. When a thin crystalline Ge film is formed on Si (111), Mn atoms travel through the Ge layer and interact with Si substrate and exhibit the magnetic properties of $Mn_5Ge_xSi_{3-x}$. On the other hand, for amorphous Ge film, Mn_5Ge_3 thin film is formed on the surface. The distribution of Mn atoms inside the Ge layer is affected by the crystallinity and roughness of the Ge layer. Temperature-dependent ferromagnetic resonance measurements reveal a relatively narrow FMR line at high temperatures, whereas the peak width and the g-value rise gradually, which are mainly associated with the enhancement of orbital angular momentum in the surface of the ferromagnetic thin film.

Acknowledgement

This work was supported in part by Scientific Research Projects Coordination Unit of Gebze Technical University (Project number: 2017-A-102-22).

References

[1] Tang JS, Wang CY, Chang LT, Fan YB, Nie TX et al. Electrical spin injection and detection in Mn5Ge3/Ge/Mn5Ge3 nanowire transistors. Nano Letters 2013; 13 (9): 4036-4043.

[2] Hamaya K, Fujita Y, Yamada M, Kawano M, Yamada S et al. Spin transport and relaxation in germanium. Journal of Physics D-Applied Physics 2018; 51 (39): 393001.

[3] Zhou Y, Han W, Chang LT, Xiu FX, Wang MS et al. Electrical spin injection and transport in germanium. Physical Review B 2011; 84 (12): 125323.

[4] Park YD, Hanbicki AT, Erwin SC, Hellberg CS, Sullivan JM et al. A group-IV ferromagnetic semiconductor: MnxGe1-x. Science 2002; 295 (5555): 651-654.

[5] Portavoce A, Abbes O, Rudzevich Y, Chow L, Le Thanh V et al. Manganese diffusion in monocrystalline germanium. Scripta Materialia 2012; 67 (3): 269-272.

[6] Zhou SQ, Schmidt H. Mn-doped Ge and Si: A review of the experimental status. Materials 2010; 3 (12): 5054-5082.

[7] Wang Y, Zou J, Zhao ZM, Han XH, Zhou XY et al. Direct structural evidences of Mn(11)Ge(8) and Mn(5)Ge(2) clusters in Ge(0.96)Mn(0.04) thin films. Applied Physics Letters 2008; 92 (10): 101913.

[8] Ozer MM, Thompson JR, Weitering HH. Growth and magnetic properties of Mn-doped germanium near the kinetic solubility limit. Physical Review B 2012; 85 (12): 125208.

[9] Toydemir B, Onel AC, Ertas M, Colakerol Arslan L. Dependence of magnetic properties on the growth temperature of Mn0.04Ge0.96 grown on Si (001). Journal of Magnetism and Magnetic Materials 2015; 374: 354-358.

[10] Guchhait S, Jamil M, Ohldag H, Mehta A, Arenholz E et al. Ferromagnetism in Mn-implanted epitaxially grown Ge on Si(100). Physical Review B 2011; 84 (2): 024432.

[11] Zhou SQ, Burger D, Li L, Skorupa W, Helm M et al. Ferromagnetic Ge:Mn prepared by ion implantation and pulsed laser annealing. In: Physics of Semiconductors: 30th International Conference on the Physics of Semiconductors 2011; 1399 (1): 699-700

[12] Passacantando M, Ottaviano L, Grossi V, Verna A, D'Orazio F et al. Magnetic response of Mn-doped amorphous porous Ge fabricated by ion-implantation. Nuclear Instruments & Methods in Physics Research Section B-Beam Interactions with Materials and Atoms 2007; 257: 365-368.

[13] Zeng L, Cao JX, Helgren E, Karel J, Arenholz E et al. Distinct local electronic structure and magnetism for Mn in amorphous Si and Ge. Physical Review B 2010; 82 (16): 165202.

[14] Verna A, Ottaviano L, Passacantando M, Santucci S, Picozzi P et al. Ferromagnetism in ion implanted amorphous and nanocrystalline MnxGe1-x. Physical Review B 2006; 74 (8): 085204.

[15] Guchhait S, Jamil M, Ohldag H, Mehta A, Arenholz E et al. Ferromagnetism in Mn-implanted epitaxially grown Ge on Si(100). Physical Review B 2011; 84 (2): 024432.

[16] Jaeger C, Bihler C, Vallaitis T, Goennenwein STB, Opel M et al. Spin-glass-like behavior of Ge: Mn. Physical Review B 2006; 74 (4): 045330.

[17] Hwang JI, Osafune Y, Kobayashi M, Ebata K, Ooki Y et al. Depth profile study using x-ray photoemission spectroscopy of Mn-doped GaN prepared by thermal diffusion of Mn. Physics of Semiconductors, Pts A and B 2007; 893 (1): 1225-1226.

[18] Kim HS, Cho YJ, Kong KJ, Kim CH, Chung GB et al. Room-temperature ferromagnetic Ga1-xMnAs (x <= 0.05) nanowires: dependence of electronic structures and magnetic properties on Mn content. Chemistry of Materials 2009; 21 (6): 1137-1143.

[19] Lungu GA, Stoflea LE, Tanase LC, Bucur IC, Radutoiu N et al. Room temperature ferromagnetic Mn: Ge(001). Materials 2014; 7 (1): 106-129.

[20] Irizawa A, Yamasaki A, Okazaki M, Kasai S, Sekiyama A et al. Bulk-sensitive photoemission of Mn5Si3. Solid State Communications 2002; 124 (1-2): 1-5.

[21] Hirsch K, Zamudio-Bayer V, Rittmann J, Langenberg A, Vogel M et al. Initial- and final-state effects on screening and branching ratio in 2p x-ray absorption of size-selected free 3d transition metal clusters. Physical Review B 2012; 86 (16): 165402.

[22] Yasasun BT, Onel AC, Aykac IG, Gulgun MA, Arslan LC. Effect of Ge layer thickness on the formation of Mn5Ge3 thin film on Ge/Si (111). Journal of Magnetism and Magnetic Materials 2019; 473: 348-354.

[23] Kassim J, Nolph C, Jamet M, Reinke P, Floro J. Mn solid solutions in self-assembled Ge/Si (001) quantum dot heterostructures. Applied Physics Letters 2012; 101 (24): 242407.

[24] Er AO, Elsayed-Ali HE. Electronically enhanced surface diffusion during Ge growth on Si(100). Journal of Applied Physics 2011; 109 (8): 084320.

[25] Gajdzik M, Surgers C, Kelemen MT, Von Lohneysen H. Strongly enhanced Curie temperature in carbon-doped Mn5Ge3 films. Journal of Magnetism and Magnetic Materials 2000; 221 (3): 248-254.

[26] Liu XB, Altounian Z. Magnetocaloric effect in Mn5Ge3-xSix pseudobinary compounds. Journal of Applied Physics 2006; 99 (8): 08Q101.

[27] De Padova P, Olivieri B, Mariot JM, Favre L, Berbezier I et al. Ferromagnetic Mn-doped Si0.3Ge0.7 nanodots self-assembled on Si(100). Journal of Physics-Condensed Matter 2012; 24 (14): 142203.

[28] Truong A, Watanabe AO, Sekiguchi T, Mortemousque PA, Sato T et al. Evidence of a perpendicular magnetocrystalline anisotropy in a Mn5Ge3 epitaxial thin film revealed by ferromagnetic resonance. Physical Review B 2014; 90 (22): 224415.

[29] Toydemir B, Onel AC, Ertas M, Arslan LC. Dependence of magnetic properties on the growth temperature of Mn0.04Ge0.96 grown on Si (001). Journal of Magnetism and Magnetic Materials 2015; 374: 354-358.

[30] Kalvig R, Jedryka E, Aleshkevych P, Wojcik M, Bednarski W et al. Ferromagnetic resonance in Mn5Ge3 epitaxial films with weak stripe domain structure. Journal of Physics D-Applied Physics 2017; 50 (12): 125001.

[31] Nakajima N, Koide T, Shidara T, Miyauchi H, Fukutani I et al. Perpendicular magnetic anisotropy caused by interfacial hybridization via enhanced orbital moment in Co/Pt multilayers: magnetic circular x-ray dichroism study. Physical Review Letters 1998; 81 (23): 5229-5232.

[32] Matveev KA, Glazman LI, Larkin AI. G-factors of discrete levels in nanoparticles. Physical Review Letters 2000; 85 (13): 2789-2792.